Selective Bundling of Zigzag Single-Walled Carbon Nanotubes

Carolin Blum,[†] Ninette Stürzl,[†] Frank Hennrich,[†,*] Sergei Lebedkin,[†] Sebastian Heeg,[‡] Heiko Dumlich,[‡] Stephanie Reich,[‡] and Manfred M. Kappes[†,§]

[†]Institut für Nanotechnologie, Karlsruhe Institute of Technology, D-76021 Karlsruhe, Germany, [‡]Institut für Experimentalphysik, Freie Universität Berlin, D-14195 Berlin, Germany, and [§]Institut für Physikalische Chemie, Karlsruhe Institute of Technology, D-76128 Karlsruhe, Germany

ABSTRACT A simple, high throughput fractionation procedure for aqueous/SDS (sodium dodecyl sulfate) suspensions of single-walled carbon nanotubes (SWNTs) is presented, which yields thin bundles of semiconducting-SWNTs with small chiral angles. To demonstrate this we show the photoluminescence signatures of nanotube suspensions that contain almost exclusively zigzag and near-zigzag tubes. Starting suspensions and resulting fractions were characterized using optical absorption, resonance Raman and photoluminescence spectroscopies as well as scanning force microscopy. Taken together with literature observations, our findings suggest that near zigzag edge tubes of similar diameters in a bundle are harder to separate from each other than for other chiral index combinations. We discuss the implications of these observations for SWNT growth and dispersion.

KEYWORDS: zigzag carbon nanotubes · bundles · gel filtration · size exclusion chromatography · separation · sorting · purification

The development and application of separation techniques for the fractionation of single-walled carbon nanotube materials (SWNTs) has become an active research field in recent years. It is driven by the fact that no known synthesis method allows the growth of nanotube samples having preselected electronic type (metallic (m) or semiconducting (s)), diameter, and chiral index. In fact, m- and s-SWNTs are typically grown together in a complex mixture of many different structures (described by a distribution of chiral indices (*n, m*)).

Fractionation of m- from s-SWNTs is an important, applications-oriented part of this separation effort and enrichment of m- *versus* s-SWNTs has in fact been achieved by various techniques including (AC) dielectrophoresis,[1] density gradient centrifugation[2] (DGC), and agarose gel electrophoresis.[3] A review article on separation methods in general, including separation of m- from s-SWNTs, gives a good overview of efforts to date.[4]

Recently, it has been shown that a procedure based on gel filtration/size exclusion chromatography methods allows high throughput separation of m- from s-SWNTs when using aqueous sodium dodecyl sulfate (SDS) starting suspensions.[5,6] Conveniently, such starting suspensions can be prepared without a centrifugation step. Size exclusion chromatography (SEC) is known to separate nanoscale objects passing through a column according to differences in their size and has been extensively used to *size-separate* SWNTs. In this sense the observation of m- *versus* s-SWNTs separation using size exclusion chromatography methods was unexpected. It turns out that the procedure relies on the initial dispersion/sonication step, which itself is already selective with respect to electronic structure type. In fact, aqueous SDS starting suspensions obtained after sonication of SWNT raw soot were found to contain s-SWNTs primarily in the form of bundles, whereas metallic SWNTs were predominantly suspended as individual tubes. With the gel filtration procedure, the bundles can then be separated from the individual tubes simply on the basis of differences in their size. By choosing an appropriate column medium, particle size, gel porosity, and eluant composition it is possible to run the SEC column as a "filter" which traps the longer, rigidly bundled s-SWNTs, whereas the smaller individualized m-SWNTs elute as expected for regular SEC. Specifically, for high throughput m/s-SWNT separation, the starting SWNT suspension is first loaded onto the column and then partly eluted with 1 wt % of SDS in water. This removes the shorter (individualized) metallic tubes, whereas bundled s-SWNTs remain trapped at the top of the column. The latter are then also removed by changing the eluant from 1 wt % SDS in H_2O to 1 wt % SChol (sodium cholate hydrate) in H_2O—whereupon the trapped semiconducting bundles partially dissolve and (completely) elute.

On the basis of these findings, we have further explored the origin, composition, and properties of s-SWNT bundles observed in the aqueous SDS starting suspensions used for high throughput m/s-SWNT separation. In the

* Address correspondence to frank.hennrich@kit.edu.

Received for review December 8, 2010 and accepted March 15, 2011.

Published online ■■■
10.1021/nn1033746

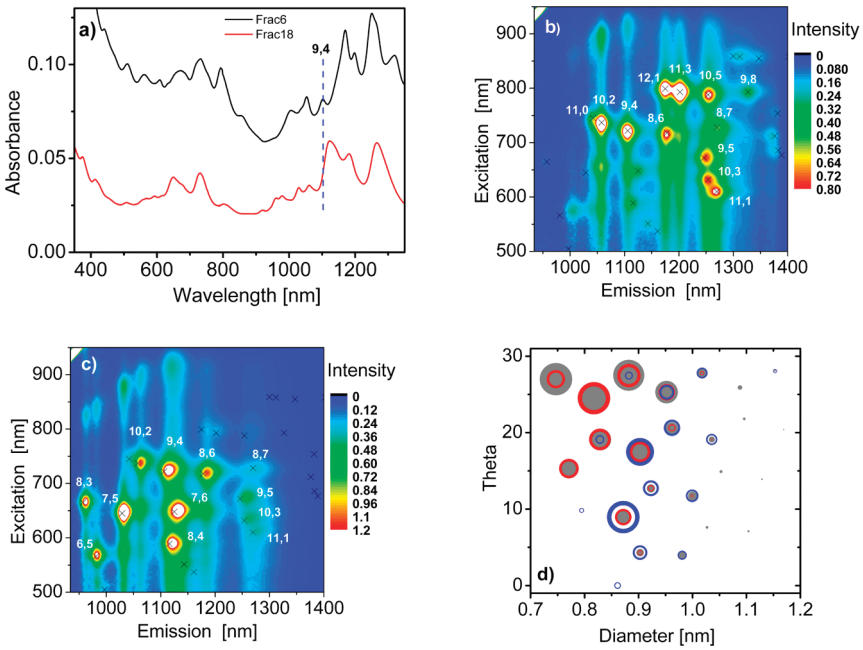

Figure 1. UV−vis−NIR absorption spectra of two fractions, 6 and 18, eluted with 2 wt % SChol in H_2O during gel filtration of HiPco SWNTs (a); these fractions are representative for the two different s-SWNT populations observed (see text); PLE maps of fraction 6 (b) and fraction 18 (c); theta/diameter plots as extracted from PLE spectra (d) of fraction 6 (area of blue circle data points indicates relative abundance under the assumption of uniform integral PLE cross sections), fraction 18 (red circles), and from a HiPco SCholate reference sample (gray circle) for comparison (see also Supporting Information for further PLE maps and absorption spectra).

present contribution, we demonstrate that such bundling appears to be particularly pronounced for tubes near the zigzag edge. This in turn allows simple fractionation of such SWNTs from the total s-SWNT population. We discuss the implications of these observations for processes occurring during SWNT growth and/or during sonication of SWNT raw materials in SDS/H_2O.

RESULTS AND DISCUSSION

As outlined above, high throughput m- *versus* s-SWNT separation using our gel filtration method involves two steps. An initial 1 wt % SDS in H_2O elution removes the metallic tubes, whereupon changing the eluant to 2 wt % SChol in H_2O then elutes the s-SWNTs.

Looking more closely, one observes that upon SChol addition, the dark "s-SWNTs" band initially localized at the top of the column evolves into two separate colored bands (see Figure S1 in Supporting Information), which move through the gel with different velocities. This is also clearly shown by the corresponding chromatogram as detected by measuring integrated SWNT G-mode Stokes−Raman intensities as a function of elution time (see Figure S2 in Supporting Information). Two separate s-SWNTs bands were observed for both PLV and HiPco materials. In the following we present additional measurements for each of the two SWNT materials in turn—first concentrating on HiPco SWNTs.

Fractions of ~1 mL were collected from both bands as they eluted from the column and were then analyzed with UV−vis−NIR absorption spectroscopy and by measuring PLE maps. Figure 1 a shows absorption spectra of fractions typical for each band: fraction 6 was collected from the first band and fraction 18 was collected from the second band. There are significant differences between both absorption spectra which implies that the (*n, m*)-distribution of both fractions is different. This becomes more obvious by comparing the corresponding PLE maps. Figure 1 panels b and c show the PLE maps of fractions 6 and fraction 18, respectively. Finally, Figure 1d shows chiral angle(theta)/diameter plots extracted from the PLE spectra of fractions 6 (blue circles) and 18 (red circles) as well as a corresponding plot for a HiPco SCholate reference sample (gray). Whereas the (*n, m*)-composition of fraction 18 is comparable to what was measured for the reference sample, the (*n, m*)-composition obtained for fraction 6 is completely different. Compared to the reference sample and fraction 18, fraction 6 is enriched in tubes with larger diameter and smaller theta (additional absorption spectra and PLE maps supporting these conclusions are shown in Supporting Information).

The SEC gel is specified by the manufacturer to separate molecules with a molar mass in the range of 5×10^3 to 2.5×10^5 g/mol. From AFM studies, the individualized SWNTs observed after spin-coating deposition of starting suspensions have an average length of 300 nm, which corresponds to a molar mass of 2×10^5 to 5×10^5 g/mol, depending on the diameter of the tube. Consequently, the latter value is already at the upper limit of the (size exclusion) fractionation range of the gel. Bundles were

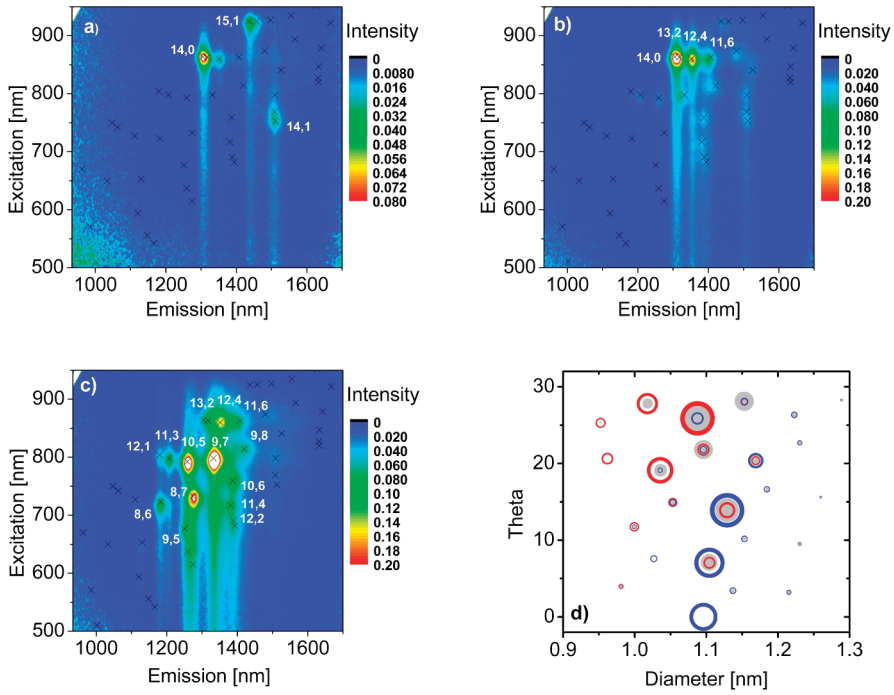

Figure 2. PLE maps of various fractions eluted upon gel filtration of PLV SWNTs: (a) integral measurement of early fractions 1−4, after concentration *via* DGC, (b) fraction 5, (c) fraction 12, and (d) theta/diameter plots as extracted from PLE spectra of fractions 5 (red circles) and 12 (blue circles), as well as from a PLV SCholate reference sample (gray circles) for comparison (see also Supporting Information for further PLE maps and absorption spectra).

found to be longer and clearly above this specified molar mass range. Consequently, they would not be expected to be able to enter the pores of the SEC medium. Instead of eluting however they appear to be so large that they nonspecifically adsorb onto the gel particles when in the presence of SDS/H_2O. After adding 2 wt % SChol in H_2O they apparently become partly dissolved and start to move through the gel in two separate bands.

The UV−vis−NIR spectra of fractions 6 and 18 show that the (9, 4)-tube can be detected in both bands. However, a comparison of the corresponding PL intensities and absorptions shows that the relative (9, 4) PL quantum yield is three times larger for fraction 18 than for fraction 6. This is consistent with a higher bundle content for the latter fraction.[7−9]

From this (and from complementary information discussed below for PLV samples) we infer that upon SChol elution the faster moving band comprises s-SWNT bundles, whereas the slower band consists primarily of individual semiconducting tubes (and some very small bundles). Together with the (*n, m*)-composition of the two separate bands this implies that s-SWNTs with larger diameters and smaller theta have a much stronger tendency to elute in bundle form. Under these conditions (SChol/H_2O), the gel seems to be working more like a normal size exclusion medium in the sense that larger bundles move through the gel more quickly than individual tubes or smaller bundles.

Compared to a HiPco SDS suspension, the PLV SDS suspension (consisting of on-average larger diameter SWNTs) behaves similarly during gel filtration: after removing the m-SWNTs and changing the eluant from 1 wt % SDS to 2 wt % SChol in H_2O, the s-SWNTs subsequently elute and evolve into two separate multicoloured bands. Furthermore, PLE maps measured for eluting fractions show a trend similar to that obtained for the HiPco material: bundles which elute first from the column are enriched in (*n, m*)-species having small theta.

Figure 2 contains PLE maps of corresponding semiconducting-SWNT fractions obtained upon gel filtration of the PLV SWNTs suspension. Note, that for the earliest SEC fractions (1−4), the nanotube concentrations were so small that in order to get enough PL intensity for a PLE map it was necessary to add several consecutive fractions together and then to concentrate them with DGC. The latter procedure does not significantly change the overall (*n, m*)-composition of the summed fractions (see Supporting Information). PLE measurements then indicated that the early fractions contained mainly the (14, 1), (15, 1), and (14, 0)-tubes. In contrast, (see also Supporting Information) more and more tubes with smaller diameters and larger theta were observed in the later fractions.

In addition to performing optical spectroscopy on early fractions 1−4, fraction 5 was immediately investigated by AFM upon elution. Figure 3 shows the corresponding height distributions. Clearly, this fraction consists primarily of bundles having an average diameter of *ca.* 4 nm. In the Supporting Information (Figure S9) we also show an analogous AFM measurement obtained for the sum of all

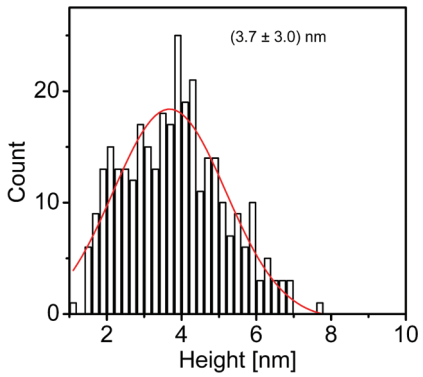

Figure 3. Height distribution as determined by intermittent contact mode AFM imaging for fraction 5 eluted upon gel filtration of PLV SWNTs. See Supporting Information for typical AFM images obtained upon spin-coating the corresponding dispersion fraction onto a silicon wafer.

column eluted s-SWNT fractions (*i.e.*, both bands together). This shows predominantly individual tubes and small bundles. Note that the fractions comprising s-SWNT bundles (*e.g.*, fraction 5) demonstrated a relatively fast (within a few weeks) formation and precipitation of large nanotube aggregates, as compared to notably more stable fractions with individual tubes. Interestingly, the PL could also be observed from precipitated, several-micrometer-large s-SWNT aggregates, albeit of a relatively weak intensity (Supporting Information, Figure S11).

Figure 4 shows a contour plot of the Raman amplitude for fraction 7 as a function of excitation energy and RBM frequency. The transition energies obtained from the resonance profiles depicted agree well with values previously reported for isolated tubes (or small bundles) in solution.[10] The intensities (amplitudes of the corresponding Raman resonance profiles) confirm the enrichment of nanotubes belonging to the $2n + m = 28$ family; in particular, the presence of the (14, 0)-tube is unequivocally confirmed. Furthermore minor contributions from other nanotube families are seen as indicated in the RRS-map.

In conclusion, our measurements show that for both HiPCo and PLV raw materials, ultrasonication in SDS/H_2O followed by a two-step gel SEC filtration procedure, yields two resolvable s-SWNT bands. The faster of these comprises bundles enriched in zigzag SWNTs as well as in tubes near the zigzag edge. There are in principle three possible origins for such bundles: (i) they are already formed during SWNT growth and survive dispersion/fractionation, (ii) they are generated during dispersion of the SWNT raw material *via* selective reassembly of individualized tubes, or (iii) they are not yet present in the starting suspensions but assemble (and then elute) during the column fractionation procedure. To differentiate between these pictures, we next discuss the relevant interaction energies.

Semiconducting SWNTs are less efficiently suspended in water/SDS during ultrasonication than m-SWNTs.[5,10] This is related to electronic-structure-type dependent differences in tube−tube and tube−SDS interaction potentials. SDS appears to be more strongly adsorbed onto m-SWNTs than s-SWNTs. Furthermore, suspended m-SWNTs have a higher packing density of SDS on their surfaces, relative to s-SWNTs.[11] Some insight may be derived from calculations of related interactions of DNA with nanotube surfaces.[12] In these, the polarizability of the nanotube surface had to be included in order to explain selective separations using DNA oligonucleotide wrapping. Niyogi *et al.* have also invoked polarizability to rationalize their observation that effective tube−tube separations can be varied by tuning SDS adsorption onto SWNTs *via* NaCl addition. The latter effect can also be used to yield diameter-dependent fractionation of m- and s-SWNTs.[14]

Overall, the differing adsorption behavior of SDS on m-*versus* s-SWNTs results from the polarizability of the nanotube surface, which is higher for metallic nanotubes. This permits an approaching point charge (*i.e.*, the anionic headgroup of SDS) to induce a positive image charge. This image charge will act to further screen electrostatic interactions between individual SDS molecules. Therefore more SDS molecules can be packed around a metallic tube compared to a less polarizable semiconducting tube and correspondingly the former are better stabilized in suspension. In fact, under our dispersion/ultrasonication conditions it seems that SDS cannot be packed densely enough around s-SWNTs to achieve extensive individualization under near-equilibrium conditions.

Two possible limiting dispersion scenarios can then be invoked if we assume zigzag enriched bundles to be present already in starting suspensions: (i) s-SWNTs preaggregated in the raw material remain bundled because sonication in SDS/water does not allow them to be completely individualized; that is, the process of individualization comes to a halt at a certain minimum bundle size, which depends on its specific (n, m)-content (and relative bundle cohesion) and (ii) sonication leads to all s-SWNTs initially becoming individualized but ongoing dynamical SDS adsorption/desorption processes allow them to (re)aggregate to form bundles enriched in the more strongly cohesive (n, m) s-SWNTs combinations.

Scenario (i) is supported by e-beam microdiffraction measurements of SWNT raw materials, which allow the acquisition of local (n, m)-distributions directly.[13,14] As-grown SWNT bundles often comprise nonstatistical (n, m)-distributions. In fact, depending on the SWNT synthesis method, smaller bundles consisting of only one or two (n, m) types have been observed.[16] Larger bundles of SWNTs appear to be made up of several of these smaller, chirality-defined, nanocrystalline bundles. These findings have led to speculations that SWNTs often grow in small crystalline bundles having only one or a few different chiralities.

Both scenarios can also be discussed in terms of starting suspension preparation conditions. Ultrasonication is widely used for dispersion of nanoparticle aggregates

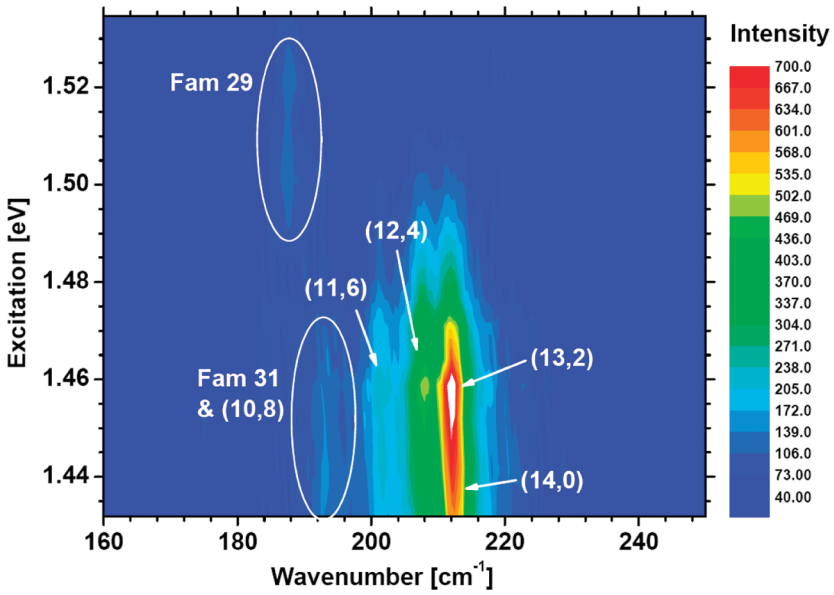

Figure 4. Contour plot of the Raman scattering intensity of fraction 7 as a function of excitation energy and radial breathing mode frequency. The four most prominent tubes, belonging to the $2n + m = 28$ family, are highlighted. Additional lower intensity signals are assigned to the respective nanotube families (see Supporting Information for a representative spectrum).

and there are several models to describe the cavitation/dispersion process. Most assume that the aggregates rupture, when the strain caused by microflows in the surrounding liquid becomes larger than the adhesive forces inside the agglomerates. Specifically, enhanced dispersion upon ultrasonication of SWNT materials is rationalized in terms of the high shear strain rates attained during cavitation. Cavitation bubble implosion can be associated with shear strain rates of up to $\sim 10^9$ s^{-1}, enough to even rupture individual SWNTs.[11] In the presence of such shear strains, exfoliation of SWNT bundles in SDS/H_2O could conceivably involve *sliding* the tubes apart. Strano *et al*. have proposed a related "unzippering" model: nanotube bundle ends first become "frayed" due to sonication; subsequently, rapid surfactant adsorption occurs at the newly accessible surfaces created between the residual bundle and individual nanotubes now dangling in solution.[15] While the individually unzipping SWNTs move relative to the bundle, surfactant continues to add along the corresponding nanotube lengths until complete separation occurs.

In such a picture of shear exfoliation, the static friction between carbon nanotubes (CNT) is obviously an important quantitiy. Using atomic/molecular mechanics, Li *et al*. showed that the interfacial shear forces required to move two structurally commensurate CNTs against each other are typically 2 orders of magnitude larger than for two incommensurate tubes.[16] In particular, the interfacial shear forces required to slide two parallel, mechanically contacting zigzag tubes apart were found to be approximately five times larger than those for two armchair tubes of roughly the same diameter. Furthermore, the interfacial shear strengths in a dimer consisting of an armchair tube and a zigzag tube (0.5−1.0 MPa) were found to be 2−3 orders of magnitude *lower* than for the commensurate dimers (A−A and Z−Z tubes).

If bundle exfoliation during ultrasonic dispersion is in fact kinetically limited by tube−tube friction, the predictions of Li *et al*. imply that zigzag tubes would be (locally) enriched in remaining microbundles, because the drag force to move two zigzag tubes against each other is much higher than that necessary for two incommensurate tubes or for two non-zigzag tubes having the same chiral index. Outside the neighborhood of cavitation bubbles, we expect s-SWNT readdition (associated with surfactant displacement) to be occurring in parallel, leading to a dynamic equilibrium. A particular consequence of such readdition might well be that bundle cores become more enriched in zigzag tubes as sonication time increases.

Experimental evidence supporting the prediction that the interaction between two zigzag tubes is stronger than between two tubes with other chiral-indices also comes from a recent study of the interaction of SWNTs with graphite/graphene. Ortolani *et al*. have reported that the surface of a few-graphene layer crystal can act as a "tangential nanosieve" when exposed to SWNTs in liquid suspension, preferentially retaining zigzag tubes on its surface.[17] This near-epitactic match of the two lattices can be monitored by directly imaging the zigzag SWNTs retained on graphene with high-resolution transmission electron microscopy and carefully analyzing their structure and substrate orientation by means of electron diffraction.

CONCLUSION

We have shown that dispersions of s-SWNT microbundles enriched in tubes with chiral indices near the zigzag edge can be prepared by a simple method based on

Sephacryl gel SEC fractionation. This makes use of starting suspensions generated by ultrasonic dispersion of SWNT raw materials in SDS/H_2O followed by prefiltration. A centrifugation step is not required. In particular, we fractionate the starting suspensions using a two-step column chromatographic separation procedure in which m-SWNTs are first eluted from the SWNT loaded column using SDS/H_2O. Under these conditions large s-SWNTs bundles much above the SEC size exclusion limit (and comparable in particle size to the column material) remain trapped at the top of the column. Upon subsequent (complete) elution of this residue with SChol/H_2O, two resolvable s-SWNT bands are observed. The faster of these comprises small bundles of s-SWNTs having chiral indices near the zigzag edge. The slower band contains a broad distribution of individual tubes with chiral indices similar to what is seen for reference dispersions (without SEC filtration).

We rationalize these observations as follows. Ultrasonic treatment of SWNT raw materials in SDS/H_2O results in (i) individualized m-SWNTs surrounded by a dense coverage of SDS molecules and (ii) large s-SWNT bundles containing regions which are locally enriched in zigzag tubes. Elution of s-SWNT bundles trapped at the top of the column using SChol/H_2O first causes individual s-SWNTs at the perimeters of these trapped bundles to be dissolved and subsequently readsorbed within the pores of the SEC column. After sufficient exfoliation, "zigzag" enriched regions are sometimes uncovered, cannot be further dissolved, and eventually become mobile as a whole, without being able to enter the column pores due to their size near the SEC exclusion limit. As a result "zigzag" enriched microbundles elute first followed by the smaller individualized s-SWNTs, as in conventional SEC.

There are some interesting implications of the above results. Standard dispersions of HiPco SWNTs in water−surfactant suspensions are assumed to contain an (*n, m*)-distribution which resembles the real (*n, m*)-distribution of the raw material. This often contains more than 20−30 different types of m- and s-SWNTs.[18] The commonly used surfactants are implicitly assumed to suspend and stabilize SWNTs in aqueous media equally well. Consequently, the (*n, m*)-distributions measured in suspension—by optical absorption, Raman mapping, and/or PLE mapping—are typically equated with the "real" integral (*n, m*)-distribution present in the SWNT raw soot.[19−21] To obtain (highly) fluorescing suspensions, the raw SWNT soot is usually treated by ultrasonication followed by an (ultra)centrifugation step to remove bundles and insoluble material. While it has already been noted that the (*n, m*)-distribution obtained after such treatments can depend somewhat on the choice of surfactant and on the pretreatment of the starting material[22,23] our findings specifically imply that semiconducting SWNTs near the zigzag edge are discriminated against when individualization protocols employing SDS/H_2O are used. Under such conditions "zigzag nanotubes" are present in the form of strongly cohesive microbundles, which are preferentially precipitated during preparation of the corresponding dispersions. It is presently unclear whether the small zigzag bundles are formed during sonication or are already present in the raw material thus reflecting locally selective catalytic growth.

METHODS

A brief description of the experimental methods is as follows. Two types of SWNT raw materials were used for this study: (i) SWNTs prepared in-house by pulsed laser vaporization (PLV) in an argon atmosphere using carbon targets doped with 1 atom % Ni and Co catalyst and an oven operated at 1000 °C[24] and (ii) HiPco SWNTs[25] as obtained from Unidym, USA.

To prepare starting suspensions. typically 10 mg of both SWNT materials was suspended in 15 mL of D_2O with 1 wt % of SDS using a tip sonicator (Bandelin, 200 W maximum power, 20 kHz, in pulsed mode with 100 ms pulses) applied for 2 h at ∼20% power. The resulting dispersion was then filtered through a Sephacryl S-1000 gel filtration medium (Amersham Biosciences) in a glass column of ∼2 cm length and 2 cm inner diameter to remove larger agglomerates. The eluted component was used as the "starting suspension" for gel filtration fractionation as described below.

Separate "reference suspensions" for HiPco as well as for PLV SWNTs were made by suspending ∼1 mg of raw SWNTs in 15 mL of D_2O with 1 wt% of SChol. After tip sonication the suspensions were centrifuged at 154.000 g for 4 h, and the upper 90% of the supernatant was carefully decanted.

Gel filtration was performed as described in ref 5 using Sephacryl S-200 gel filtration medium (Amersham Biosciences) in a glass column of 20 cm length and 2 cm inner diameter. After filling the glass column with the filtration medium, the gel was slightly compressed to yield a final height of ∼14 cm. For the separation, ∼10 mL of SWNT starting suspension was applied to the top of the column and subsequently a solution of 1 wt % SDS in H_2O as eluant was pushed through the column by applying sufficient pressure with compressed air to ensure a flow of ∼1 mL/min. As described in ref 5, after ∼10 mL of this eluant had been added most of the m-SWNTs had moved through the column, whereas the s-SWNTs remained trapped in the upper part of the gel. After applying a total of ∼20 mL of SDS solution in this fashion, the metallic tubes were completely removed from the gel. After a change of the eluant from 1 wt % SDS in H_2O to 2 wt % SChol in H_2O, the s-SWNTs also subsequently eluted completely from the column and were collected separately in fractions of ∼1 mL.

Process Raman spectra at 785 nm excitation were obtained directly at the outlet of the glass size exclusion column with a Kaiser Optical Holospec spectrograph which comprises a fiber optic probe head incorporating both excitation laser aperture and collection optics. Spectra were processed *via* the Kaiser Holoreact program package for Matlab (The Mathworks, Inc.). Peak heights of Raman features were determined at defined wavenumber (= Stokes shift) intervals over each spectrum taken. These were typically recorded every 20 s during the gel fractionation experiment. A corresponding chromatogram obtained by plotting the integrated G-mode Raman scattering intensity *versus* elution time is shown in the Supporting Information.

For spectroscopic characterization, gel filtration fractions were subsequently diluted to one-tenth of the initial concentration using D_2O/1 wt % surfactant solution. UV−vis−NIR absorption spectra of the diluted fractions were recorded on a Varian Cary 500

spectrophotometer. Photoluminescence maps were measured in the emission range of ~900 to 1700 nm and excitation range of 500 to 950 nm (scanned in 3 nm steps) using a modified FTIR spectrometer (Bruker IFS66) equipped with a liquid-nitrogen-cooled Ge-photodiode and a monochromatized excitation light source as described elsewhere.[26]

Raman resonance profiles were obtained using an HYB T64000 triple Raman spectrometer. A tunable Ti:Sa laser was used for excitation between 1.43 and 1.53 eV in steps of 5−10 meV at a laser power up to 15 mW. The Raman signal from the solution was collected through a 10× objective (NA 0.25) in backscattering configuration. We normalized the Raman intensity with respect to laser power, integration time, and spectrometer response by the nonresonant signal of CaF_2.[27] The laser lines and spectra were calibrated with a neon lamp.

AFM samples were prepared and measured as described in ref 28. In brief, samples were prepared by the spin-coating of SWNT suspensions onto silicon wafers followed by rinsing with water and acetone. Intermittent contact mode AFM images were recorded with a Digital Instruments Multimode SPM with NSC15 silicon cantilevers (MikroMasch). The heights and lengths of the objects measured were extracted from AFM pictures with the help of the Software package SIMAGIS (Smart Imaging Technologies Co.). Tube lengths were determined to within a lateral resolution of ~20 nm.

Density gradient centrifugation (DGC) was used for concentrating gel filtration fractions when necessary (see below). Typically ~3 mL suspension volumes were concentrated to ~0.1 mL using an Optima Max-E centrifuge (Beckman-Coulter) equipped with a MLA-80 fixed angle rotor and a procedure similar to that reported previously in ref 5. In short ~3 mL of the SEC suspension was overlaid onto 5 mL of water containing 60 wt % of Iodixanol (Optiprep, from Sigma) as the density gradient medium, within 8 mL of Quick-Seal polyallomer centrifuge tubes. These were then spun for 18−20 h at 15 °C and 45 000 rpm corresponding to centripetal accelerations of ~103 000 and ~140 000 g at the middle and bottom of the centrifuge tube, respectively. This resulted in a self-generated density gradient. After centrifugation for 18−20 h a small colored region (~0.1 mL) evolved within the density gradient. This colored SWNT region was then harvested in increments of ~20 μL by carefully puncturing the tube at the top and bottom and applying a slight air overpressure *via* the top hole. Concentrated fractions were then analyzed by PLE mapping (see also Supporting Informatioin).

Acknowledgment. This research was supported by the Bundesministerium für Bildung und Forschung (BMBF) as administered by POF-NanoMicro, by the Deutsche Forschungsgemeinschaft (DFG) as administered by the Center for Functional Nanostructures, the European Research Council (ERC) under Grant No. 210642 (OptNano), and the Karlsruhe School of Optics & Photonics (KSOP).

Supporting Information Available: Gel fractionation, photographs of the gel columns, Raman-derived chromatogram, absorption spectra and PLE maps of fractions; AFM images and height and length distributions; RBM Raman spectra for nanotubes in specific fractions; and PLE map of a large aggregate of s-SWNTs. This material is available free of charge *via* the Internet at http://pubs.acs.org.

REFERENCES AND NOTES

1. Krupke, R.; Hennrich, F.; von Loehneysen, H.; Kappes, M. M. Separation of Metallic from Semiconducting Single-Walled Carbon Nanotubes. *Science* **2003,** *301*, 344–347.
2. Arnold, M. S.; Green, A. A.; Hulvat, J. F.; Stupp, S. I.; Hersam, M. C. Sorting Carbon Nanotubes by Electronic Structure Using Density Differentiation. *Nat. Nanotechnol.* **2006,** *1*, 60–65.
3. Tanaka, T.; Jin, H.; Miyata, Y.; Kataura, H. High-Yield Separation of Metallic and Semiconducting Single-Wall Carbon Nanotubes by Agarose Gel Electrophoresis. *Appl. Phys. Express* **2008,** *1*, 114001−1−3.
4. Hersam, M. C. Progress Towards Monodisperse Single-Walled Carbon Nanotubes. *Nat. Nanotechnol.* **2008,** *3*, 387–394.
5. Moshammer, K.; Hennrich, F.; Kappes, M. M. Selective Suspension in Aqueous Sodium Dodecyl Sulfate According to Electronic Structure Type Allows Simple Separation of Metallic from Semiconducting Single-Walled Carbon Nanotubes. *Nano Res.* **2009,** *2*, 599–606.
6. Liu, H.; Feng, Y.; Tanaka, T.; Urabe, Y.; Kataura, H. Diameter-Selective Metal/Semiconductor Separation of Single-Wall Carbon Nanotubes by Agarose Gel. *J. Phys. Chem. C* **2010,** *114*, 9270–9276.
7. Bundles consisting of only s-SWNTs are known to exhibit photoluminescence. The authors in ref 8 were able to measure PLE maps of bundled and unbundled segments of the same—near-ideal air-suspended—SWNTs to directly reveal extra PL features arising from energy transfer (ET) processes. Apart from additional features in the PLE maps, which can be attributed to Förster resonance ET, bundling induced changes to the PL spectra were found to be very mild, even preserving line shape and line width. However emission intensity of the tubes studied was found to be approximately halved as compared to the unbundled SWNTs. Bundles are postulated to manifest reduced fluorescence because of energy transfer (ET) to neighbouring nanotubes in the bundle. The authors in ref 9 measured ET rates in the order of $\sim 10^{14}$ s^{-1}. However, details are presently unclear because ensembles of chirality controlled semiconducting SWNT bundles have not previously been available.
8. Lefebvre, J.; Finnie, P. Photoluminescence and Foerster Resonance Energy Transfer in Elemental Bundles of Single-Walled Carbon Nanotubes. *J. Phys. Chem. C* **2009,** *113*, 7536–7540.
9. Lüer, L.; Crochet, J.; Hertel, T.; Cerullo, G.; Lanzani., G. Ultrafast Excitation Energy Transfer in Small Semiconducting Carbon Nanotube Aggregates. *ACS Nano* **2010,** *7*, 4265–4273.
10. Islam, M. F.; Rojas, E.; Bergey, D. M.; Johnson, A. T.; Yodh, A. G. High Weight Fraction Surfactant Solubilization of Single-Wall Carbon Nanotubes in Water. *Nano Lett.* **2003,** *3*, 269–273.
11. Niyogi, S.; Densmore, C. G.; Doorn, S. K. Electrolyte Tuning of Surfactant Interfacial Behavior for Enhanced Density-Based Separations of Single-Walled Carbon Nanotubes. *J. Am. Chem. Soc.* **2008,** *131*, 1144–1153.
12. Lustig, S. R.; Jagota, A.; Khripin, C.; Zheng, M. Theory of Structure-Based Carbon Nanotube Separations by Ion-Exchange Chromatography of DNA/CNT Hybrids. *J. Phys. Chem. B* **2005,** *109*, 2559–2566.
13. Colomer, J.-F.; Henrard, L.; Lambin, Ph.; Van Tendeloo, G. Electron Diffraction and Microscopy of Single-Wall Carbon Nanotube Bundles Produced by Different Methods. *Eur. Phys. J. B* **2002,** *27*, 111–118.
14. Colomer, J.-F.; Henrard, L.; Lambin, Ph.; Van Tendeloo, G. Electron Diffraction Study of Small Bundles of Single-Wall Carbon Nanotubes with Unique Helicity. *Phys. Rev. B* **2001,** *64*, 125425−1−7.
15. Strano, M. S.; Moore, V. C.; Miller, M. K.; Allen, M. J.; Haroz, E. H.; Kittrell, C.; Hauge, R. H.; Smalley, R. E. The Role of Surfactant Adsorption during Ultrasonication in the Dispersion of Single-Walled Carbon Nanotubes. *J. Nanosci. Nanotechnol.* **2003,** *3*, 81–86.
16. Li, C.; Liu, Y.; Yao, X.; Ito, M.; Noguchi, T.; Zheng, Q. Interfacial Shear Strengths between Carbon Nanotubes. *Nanotechnology* **2010,** *21*, 115704-1–5.
17. Ortolani, L.; Houdellier, F.; Monthioux, M.; Morandi, V. Chirality Dependent Surface Adhesion of Single-Walled Carbon Nanotubes on Graphene Surfaces. *Carbon* **2010,** *48*, 3050–3056.
18. Bachilo, S. M.; Strano, M. S.; Kittrell, C.; Hauge, R. H.; Smalley, R. E.; Weisman, R. B. Structure-Assigned Optical Spectra of Single-Walled Carbon Nanotubes. *Science* **2002,** *298*, 2361–2366.
19. This approach is apparently a rough approximation. To accurately quantify the abundance of nanotube species in a given sample by the aforementioned optical methods (and not by comparison of different suspensions), chirality

specific properties such as electron−phonon coupling (Raman) and transition probabilities (Raman and PLE) have to be taken into account; see for example refs 20 and 21.
20. Heeg, S.; Malic, E.; Casiraghi, C.; Reich, S. Quantitative Composition of a Single-Walled Carbon Nanotube Sample: Raman Scattering *versus* Photoluminescence. *Phys Stat. Sol. (b)* **2009,** *246*, 2740–2743.
21. Jorio, A.; Fantini, C.; Pimenta, M. A.; Heller, D. A.; Strano, M. S.; Dresselhaus, M. S.; Oyama, Y.; Jiang, J.; Saito, R. Carbon Nanotube Population Analysis from Raman and Photoluminescence Intensities. *Appl. Phys. Lett.* **2006,** *88*, 023109-1–3.
22. Fantini, C.; Cassimiro, J.; Peressinotto, V. S. T.; Plentz, F.; Souza Filho, A. G.; Furtado, C. A.; Santos, A. P. Investigation of the Light Emission Efficiency of Single-Wall Carbon Nanotubes Wrapped with Different Surfactants. *Chem. Phys. Lett.* **2009,** *473*, 96–101.
23. Duque, J. G.; Nicholas, A.; Parra-Vasquez, G.; Behabtu, N.; Green, M. J.; Amanda, O. E.; Higginbotham, L.; Price, B. K.; Leonard, A. D.; Schmidt, H. K.; *et al.* Diameter-Dependent Solubility of Single-Walled Carbon Nanotubes. *ACS Nano* **2010,** *4*, 3063–3072.
24. Lebedkin, S.; Schweiss, P.; Renker, B.; Malik, S.; Hennrich, F.; Neumaier, M.; Stoermer, C.; Kappes, M. M. Single-Wall Carbon Nanotubes with Diameters Approaching 6 nm Obtained by Laser Vaporization. *Carbon* **2002,** *40*, 417–423.
25. Bronikowski, M. J.; Willis, P. A.; Colbert, D. T.; Smith, K. A.; Smalley, R. E. Gas-Phase Production of Carbon Single-Walled Nanotubes from Carbon Monoxide *via* the HiPco Process: A Parametric Study. *J. Vac. Sci. Technol. A* **2001,** *19*, 1800–1805.
26. Lebedkin, S.; Hennrich, F.; Kiowski, O.; Kappes, M. M. Photophysics of Carbon Nanotubes in Organic Polymer-Toluene Dispersions: Emission and Excitation Satellites and Relaxation Pathways. *Phys. Rev. B* **2008,** *77*, 165429-1–8.
27. Maultzsch, J.; Telg, H.; Reich, S.; Thomsen, C. Radial Breathing Mode of Single-Walled Carbon Nanotubes: Optical Transition Energies and Chiral-Index Assignment. *Phys. Rev. B* **2005,** *72*, 205438-1–16.
28. Hennrich, F.; Krupke, R.; Arnold, K.; Rojas Stuetz, J. A.; Lebedkin, S.; Koch, T.; Schimmel, T.; Kappes, M. M. The Mechanism of Cavitation-Induced Scission of Single-Walled Carbon Nanotubes. *J. Phys. Chem. B* **2007,** *111*, 1932–1937.